JOURNAL OF MATERIALS SCIENCE 28 (1993) 5783–5792

Solid-state electrochemical CO_2 gas sensors based on sodium ionic conductors

Y. SADAOKA, Y. SAKAI, M. MATSUMOTO, T. MANABE
Department of Applied Chemistry, Faculty of Engineering, Ehime University, Matsuyama 790, Japan

The sensing characteristics of a solid-state electrochemical CO_2 gas sensor, expressed as $Pt|O_2$, Na_2O || Na ionic conductor || $Na_2CO_3|CO_2$, $O_2|Pt$ were investigated in terms of a two-electron electrochemical reaction. The number of electrons for the cell reaction was higher than 2 and approached 2 with an increase in the operating temperature up to about 500 °C. The introduction of water vapour induced a lowering of the e.m.f. and a prolongation of the response time. The formation of sodium oxides in the Na_2CO_3 layer was considered as a possible cause of these water effects. The sensing characteristics recovered completely after the water vapour was cutoff. The e.m.f. reduction due to water sorption was depressed by using a densified $Na_3Zr_2Si_2PO_{12}$. A densified $Na_3Zr_2Si_2PO_{12}$-based electrolyte is preferable for use as a gas sensor with a fast response and high stability for detection of CO_2 in air.

1. Introduction

The discovery of $Na_3Zr_2Si_2PO_{12}$ represents an important development in the field of solid electrolytes because it shows the existence of a three-dimensional framework structure comparable to that of β-alumina. It has been shown that crystalline compounds with the composition $Na_{1+X}Zr_2Si_XP_{3-X}O_{12}$ belong to the group of fast sodium ion conductors. The compositions with the highest ionic conductivities are the original solid solution system with $1.8 \leq X \leq 2.4$ [1, 2]. Recently, there has been considerable interest in solid glass electrolytes [3]. Glasses have several advantages over crystalline materials for solid electrolyte and/or chemical sensor applications: ease of preparation as thin plates or thin coated elements, absence of grain boundaries and pores, and isotropy. Although various types of CO_2 gas sensor have been proposed [4–6], gas sensors based on all solid-state galvanic cells have become increasingly important in practical applications [7–13]. It has been reported that adding sodium aluminosilicate glass to $Na_3Zr_2Si_2PO_{12}$ powder is effective for fabricating a densified fast sodium ionic conductor and in decreasing the sintering temperature [14]. Densified sodium ionic conductors are preferable for fabricating all solid-state gas sensors based on a galvanic cell.

This paper presents the results of a study of several sodium ionic conductors for a solid-state electrochemical CO_2 gas sensor. The effect of water vapour on the sensing characteristics was also examined.

2. Experimental procedure

$Na_3Zr_2Si_2PO_{12}$ crystalline powder was made from reagent-grade Na_2CO_3, $NH_4H_2PO_4$, ZrO_2 and SiO_2 using conventional ceramic techniques. The raw materials were ball-milled with ethanol, dried at 100 °C, calcined in air for 4 h at 900 °C and then ground. Pellets were pressed at 1000 kg cm^{-2} and sintered in air for 15 h at 1250 °C. The powder prepared by milling was compressed again and sintered at 1000 °C (NA-1000).

Na_2O–Al_2O_3–$4SiO_2$ was made from reagent-grade Na_2CO_3, Al_2O_3 and SiO_2 by heating at between 1200 and 1350 °C. Powder was obtained by milling. A mixture of $Na_3Zr_2Si_2PO_{12}$ crystalline powder and 40 wt % Na_2O–Al_2O_3–$4SiO_2$ glass was sintered at 1000 °C for 24 h (NA-40).

A crystalline powder of $Na_5YSi_4O_{12}$ was prepared by sintering a mixture of Na_2CO_3, Y_2O_3, and SiO_2 at 1000 °C for 24 h in air, followed by milling. Na_2O–Y_2O_3–SiO_2 glass (6.69 : 1.00 : 9.95 in mole ratio) was prepared by melting the compressed powder and then quickly pouring the molten liquid on to a room-temperature copper plate. Powder was obtained by milling. A mixture of $Na_5YSi_4O_{12}$ and 20 wt % Na_2O–Y_2O_3–SiO_2 glass was then sintered at 1000 °C for 24 h (NAYSI).

Zircon-based ceramic (ZPNA-20) was a mixture of $ZrSiO_4$, Na_2HPO_4 and H_3PO_4 (100 : 0.30 : 0.37 in weight), dried at 400 °C and sintered at 1000 °C in air for 24 h. $Na_3Zr_2Si_2PO_{12}$ pellets were donated by NGK Co. Ltd (NA-NGK). Pellets were 10 mm in diameter and 0.5 mm thick.

Platinum paste, 4 mm × 4 mm, was applied to opposing faces of the pellets by painting and then heating at 800 °C. The electrical properties were measured using an LCZ meter (100 Hz–100 kHz). The sensor elements were galvanic-type cells of the following form:

$$Pt|O_2,\ Na_2O \parallel \text{Na ionic conductor} \parallel Na_2CO_3|CO_2,\ O_2|Pt \quad (1)$$

A pellet with platinum electrodes was fixed on the top of an alumina tube (10 mm in diameter) with an inorganic adhesive containing sodium. The electrode seated inside the tube acted as a reference electrode. The platinum sensing electrode was seated on the outside face of the disc, covered with Na_2CO_3, $NaHCO_3$ and NaOH and then dried at 80 °C. Standard gases, air (CO < 1 p.p.m., CO_2 < 2 p.p.m., HCl < 1 p.p.m. and H_2O < 10 p.p.m.) or CO_2 at 10, 100 and 1000 p.p.m. or 1 and 10% CO_2 diluted with air, were introduced to the working (sensing) electrode side. Air was introduced to the reference electrode side. The e.m.f. of the sensor was measured with a digital electrometer. The crystalline phases were identified at room temperature by the standard X-ray diffraction technique (XRD). The microstructures were examined using a scanning electron microscope (SEM). The deformations of electrolytes on exposure to humid air, with and without CO_2, were also examined by thermal gravimetry.

3. Results and discussion

3.1. Identification by XRD and SEM

The prepared disc-shaped electrolytes were examined by XRD; results are shown in Fig. 1. For NA-NGK and NA-1000, all the observed peaks between $10° < 2\Theta < 40°$ were assigned to $Na_3Zr_2Si_2PO_{12}$ (monoclinic). Most of the diffraction peaks assigned to $Na_3Zr_2Si_2PO_{12}$ were confirmed for NA-40 with a small signal at $2\Theta = 26.7°$ (α-quartz) that is also observed for Na_2O–Al_2O_3–SiO_2 glass alone. It seems that the $Na_3Zr_2Si_2PO_{12}$ crystals were not deformed by addition of the glass. The existence of $Na_3Zr_2Si_2PO_{12}$ crystals and $ZrSiO_4$ was observed for ZPNA-20, the content of the former being considerably less than that of the latter. NAYSI was a mixture of $Na_5YSi_4O_{12}$, $Na_3YSi_2O_7$, SiO_2 etc. and the main product was $Na_5YSi_4O_{12}$.

Fig. 2 shows some of the microstructures of electrolytes and the Pt electrode. NA-1000 sintered at 1000 °C was very porous. For NA-NGK, the densification degree was higher than that for NA-1000. ZPNA-20 showed much more developed sintering than NA-1000 and NA-NGK, but many micropores (1 μm or less in diameter) were observed. The morphology of NAYSI was considerably different from the three above-mentioned electrolytes, each particle being nearly spherical. Sintering was well advanced. The surface structure of NA-40 was clearly different from the others, i.e. the morphology of the particles was unclear as were the neck and grain boundaries. Micropores with diameters of 2–3 μm were occasionally detected and the surface density of the pores was much lower. Also, the depth of the pores was less than 2 μm. The Pt electrode was very porous while the interconnections were well developed.

3.2. Electrical properties of electrolytes

Complex-plane impedance analysis of electrolytes with Pt electrodes was used to figure out their electrical characteristics. In the frequency region between

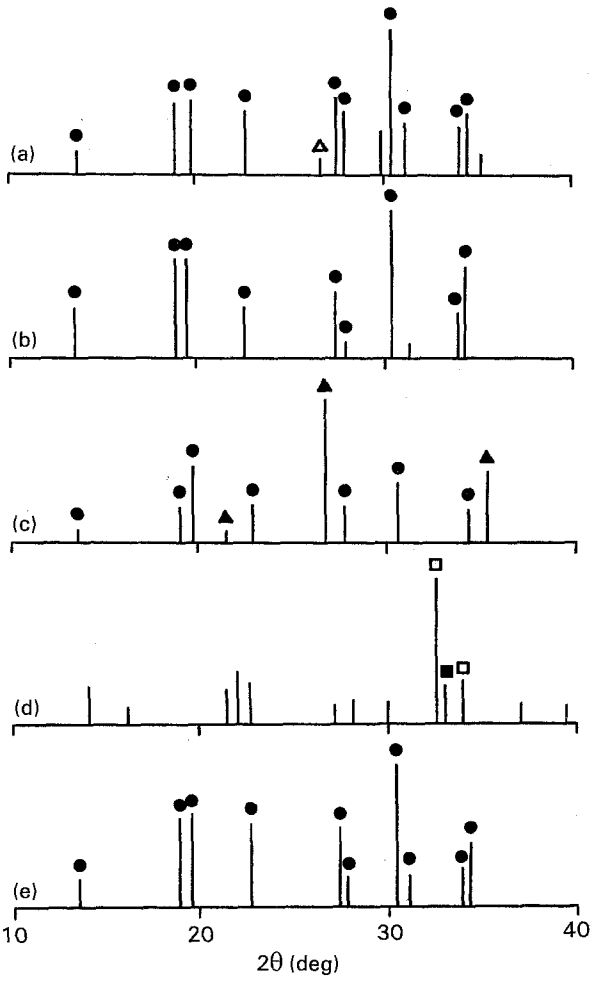

Figure 1 XRD results for electrolytes: (a) NA-40, (b) NA-NGK, (c) ZPNA-20, (d) NAYSI, (e) NA-1000; (●) $Na_3Zr_2Si_2PO_{12}$, (△) α-SiO_2, (▲) $ZrSiO_4$, (□) $Na_5YSi_4O_{12}$, (■) $Na_3YSi_2O_7$.

100 Hz and 100 kHz, only quasi-straight lines were observed at 100 °C or higher. From these observed results the conductivity component at each temperature was derived from an extrapolation to zero reactance (Z'') of the impedance plot. The conductivity data were characterized by the Arrhenius equation

$$\sigma T = \sigma_0 \exp(-E/kT) \quad (2)$$

where σ is the conductivity, σ_0 is the pre-exponential factor, E the activation energy, k the Boltzmann constant and T the absolute temperature.

For some electrolytes, the activation energy for the ionic conductivity changes at a critical temperature (T_c). For NA-40, the relation between σT and $1/T$ is expressed by an equation with a constant activation energy, as already reported [14]. The results obtained are summarized in Table I. The resistivity of the solid electrolytes was enhanced by exposure to CO_2 and/or H_2O. The resistivity at 100 °C observed in air with H_2O vapour was about three-fold higher than that observed in air for NAYSI. The coexistence of 10% CO_2 induced a further enhancement of the resistivity. Similar effects of H_2O vapour and CO_2 gas on the resistivity were also observed for NA-40, i.e. the resistivities at 100 °C observed in air with H_2O vapour or with H_2O and CO_2 were about 2 to 2.5 times higher than that in dry air. For both samples, the resistivity

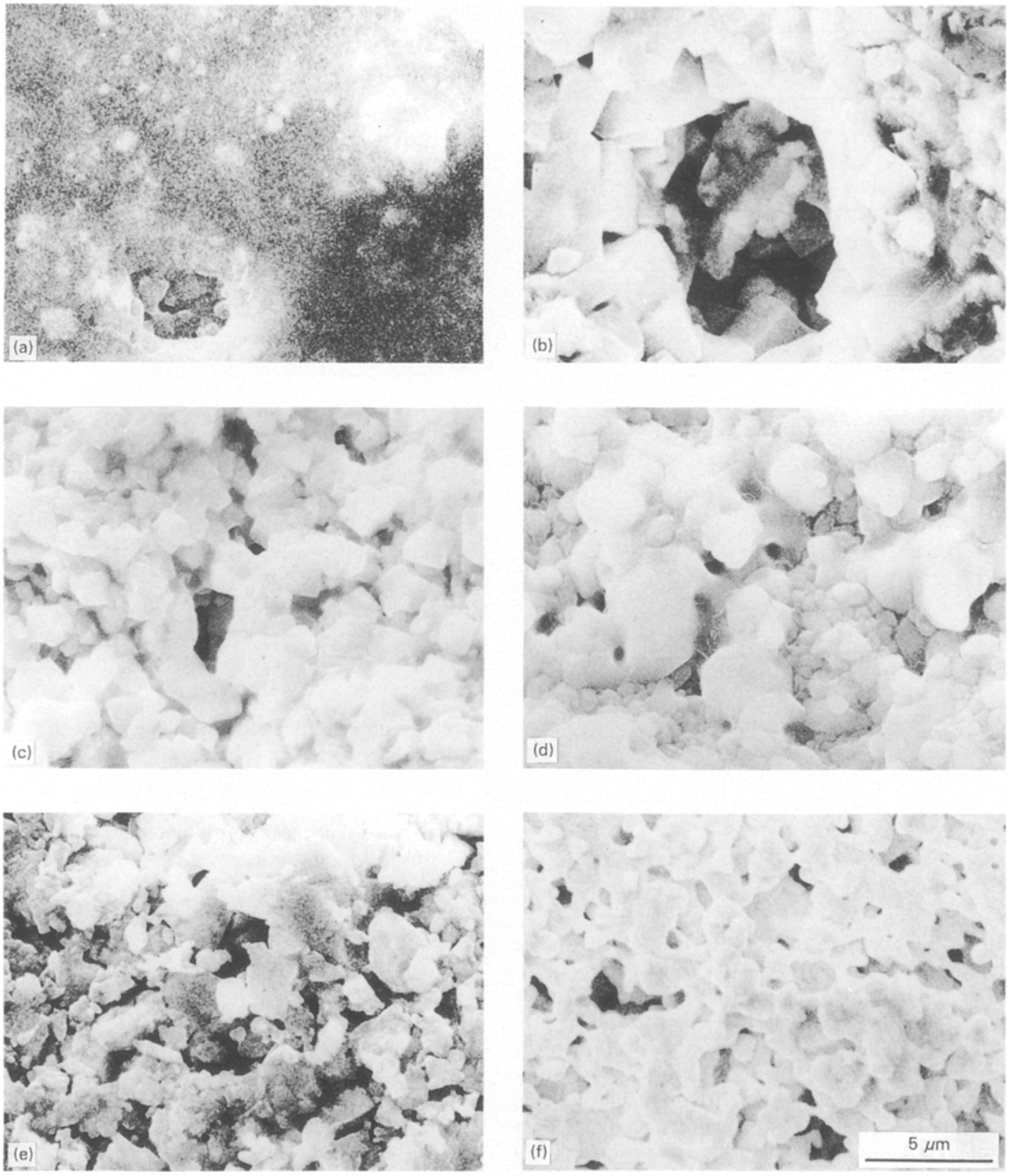

Figure 2 SEM photographs of electrolytes and Pt electrode formed on the electrolyte: (a) NA-40, (b) NA-NGK, (c) ZPNA-20, (d) NAYSI, (e) NA-1000 (f) Pt electrode.

was almost completely recovered in air when the sample was heated to 300 °C or higher.

The formation of NaOH, $NaHCO_3$ and Na_2CO_3, on exposure to humid air containing CO_2, is probably responsible for the enhancements in resistivity. It is known that the conductivity of a sodium ionic conductor such as β-alumina decreases when the sample is exposed to moisture in the presence of carbon dioxide [15]. A hydrated surface region is formed and sodium ions react with the water layer to form a hydrated sodium hydroxide. The sodium hydroxide formed reacts with CO_2 and produces Na_2CO_3, $NaHCO_3$ etc. For β-alumina, the evolution of water and carbon dioxide continues during the heating process up to 200 °C and up to 600 °C, respectively. As mentioned, the conductivity of NA-40 and NAYSI exposed to moisture containing carbon dioxide can be recovered by heat treatment at 300 °C or higher. It seems that most of the carbonate decomposes to sodium oxides in dry air without carbon dioxide.

3.3. Thermogravimetric analysis of electrolytes

Thermogravimetrical behaviour was also affected by the electrolyte's history. Thermodynamically, the formation of NaOH, $NaHCO_3$ and Na_2CO_3 is possible when the solid electrolyte is exposed to water vapour and/or CO_2. It is well known that NaOH is a

TABLE I Electrical characteristics of electrolytes

Sample	E_H (eV)	E_L (eV)	σ at 573 K ($S\,cm^{-1}$)	T_C (K)
NA-40	0.390		9.2×10^{-4}	–
ZPNA-20	0.223	0.286	1.4×10^{-2}	463
NA-1000	0.271	0.298	1.3×10^{-2}	523
NAYSI	0.212	0.258	1.2×10^{-1}	473

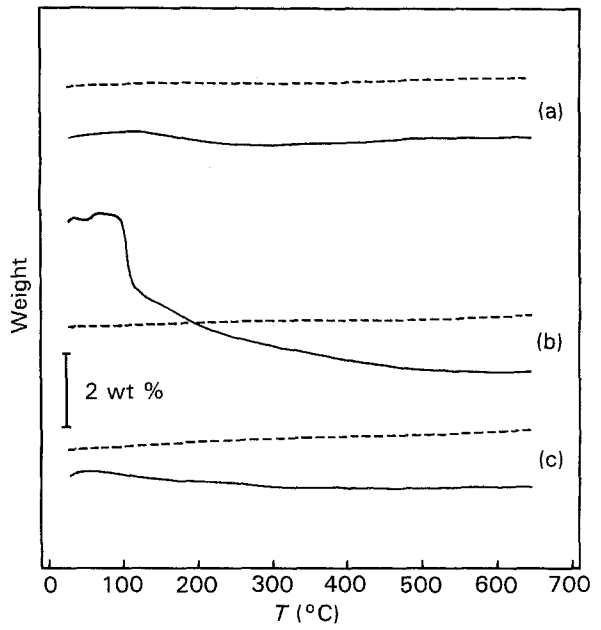

Figure 3 Weight loss curves of (---) ZPNA-20 and (—) NAYSI powders in dry air: (a) after heating at 650 °C in dry air, (b) after exchanging the ambient atmosphere from dry air to humid air with 10% CO_2 at 650 °C, (c) after the measurement of (b).

strong CO_2 getter and results in $NaHCO_3$. The formation of Na_2CO_3 follows the thermal decomposition of $NaHCO_3$, when $NaHCO_3$ is held at 270 °C or more. It is well known that the decomposition temperature of Na_2CO_3 is 850 °C. Fig. 3 shows the weight loss curves for the powdered electrolytes. As a pretreatment, the freshly prepared NAYSI powder was heated in dry air up to 650 °C. After cooling to room temperature in dry air, the first run was done in dry air. In this measurement, no distinct weight losses were observed (curve (a) in Fig. 3). The second run was done in dry air, after exchanging the ambient atmosphere from air to humid air with 10% CO_2 at 650 °C and after exchanging to dry air at room temperature. A steep weight loss was observed at around 100 °C and a gradual decrease in weight continued up to 400 °C (curve (b)).

It seems that the weight loss observed at around 100 °C is caused by desorption of the adsorbed water. The decreases observed in a higher temperature range may be caused by the decomposition of $NaHCO_3$ but also Na_2CO_3, since the weight loss continued up to 500 °C or higher. For the samples heated at 650 °C in dry air, no weight losses were observed (curve (c) in Fig. 3). The formation of sodium compounds may be limited to the surfaces of the particles. For the powdered ZPNA-20 pretreated at 650 °C in dry air, no distinct weight losses were recorded for the electrolyte exposed to humid air or humid air with 10% CO_2. A similar result was also confirmed for NA-1000. It seems that ZPNA-20, NA-40 and NA-1000 are more stable than NAYSI, i.e. the formation of NaOH or $NaHCO_3$ by exposure to H_2O vapour is depressed for NASICON-based ceramics rather than for NAYSI.

3.4. Thermodynamically interpreted sensing characteristics

A cell fabricated with electrolytes will respond to the difference in chemical potentials of sodium at the electrodes. The electrochemical potential is the sum of the chemical and electric potentials:

$$\mu'Na + F\Phi' = \mu''Na + F\Phi'' \quad (3)$$

where μ and Φ denote the chemical and electrical potential, respectively, F is the Faraday constant and single and double primes denote anode and cathode, respectively. The open-circuit e.m.f. E is the difference in electrical potentials at the electrodes:

$$E = \frac{\mu'Na - \mu''Na}{F} = \Phi'' - \Phi'$$

$$= \frac{RT}{F} \ln \frac{a'}{a''} \quad (4)$$

where a denotes the sodium activity. For the cell, expressed as

$$O_2, Pt \parallel \text{electrolyte} \parallel Pt, Na_2CO_3, CO_2, O_2$$

it is assumed that the chemical potential at the anode is controlled by the reaction

$$Na_2CO_3 \rightarrow 2Na^+ + CO_2 + \tfrac{1}{2} O_2 + 2e^- \quad (5)$$

and that at the cathode by the equation

$$2Na^+ + \tfrac{1}{2} O_2 + 2e^- \rightarrow Na_2O \quad (6)$$

The overall reaction is predicted to be

$$Na_2CO_3 \rightarrow Na_2O + CO_2 \quad (7)$$

The e.m.f. of the cell is then expected to be

$$E = -\left[\frac{\Delta G(Na_2O) + \Delta G(CO_2) - \Delta G(Na_2CO_3)}{2F}\right]$$

$$- \frac{RT}{2F} \ln [a(Na_2O)P(CO_2)] \quad (8)$$

where $\Delta G(i)$ is the standard free energy of formation and $P(i)$ the concentration of species i. If the activity of Na_2O is constant, the e.m.f. gives the concentration of CO_2. The theoretical sensitivity (ΔE_T in mV per decade) for CO_2, estimated from the assumed two-electron electrochemical reaction, is noted in Table II.

Thermodynamically, the formation of NaOH, $NaHCO_3$ and Na_2CO_3 is considered for a solid electrolyte exposed to water vapour and/or CO_2. The possible reactions are as follows:

$$Na_2O + H_2O \rightarrow 2NaOH$$

$$Na_2O_2 + CO_2 + H_2O \rightarrow NaHCO_3 + NaOH$$

$$NaOH + \tfrac{1}{2}CO_2 \rightarrow \tfrac{1}{2} Na_2CO_3 + \tfrac{1}{2} H_2O$$

TABLE II Sensing characteristics of sensors with Na_2CO_3 layer

Temperature (°C)	ΔE_T	NA-40		NA-NGK		ZPNA-20		NA-1000		NAYSI	
		ΔE_A (mV)	ΔE (mV)	ΔE_A (mV)	ΔE (mV)	ΔE_A (mV)	ΔE (mV)	ΔE_A (mV)	ΔE (mV)	ΔE_A (mV)	ΔE (mV)
370	64	131	45	–	–	105	49	0	0	–	–
400	67	145	51	–	–	–	–	–	–	–	–
420	69	155	60	–	–	128	66	–	–	–	–
430	70	–	–	122	70	–	–	–	–	–	–
470	74	168	70	114	74	127	72	0	0	131	71
500	77	156	75	113	77	–	–	–	–	–	–
520	79	–	–	–	–	121	75	–	–	–	–

ΔE_T = expected value from a two-electron reaction where $\Delta E_A = E_{air} - E_{100\ p.p.m.}$; $\Delta E = E_{100\ p.p.m.} - E_{1000\ p.p.m.}$, Reference = dry air (< 2 p.p.m. CO_2).

$$NaOH + CO_2 \rightarrow NaHCO_3$$

$$NaHCO_3 + \tfrac{1}{2} Na_2O \rightarrow Na_2CO_3 + \tfrac{1}{2} H_2O$$

$$NaHCO_3 + \tfrac{1}{2} Na_2O_2 \rightarrow Na_2CO_3 + \tfrac{1}{2} H_2O + \tfrac{1}{4} O_2$$

$$2NaHCO_3 \rightarrow Na_2CO_3 + H_2O + CO_2$$

NaOH can be easily removed as a result of reactions with CO_2. The formation of Na_2CO_3 from $NaHCO_3$ occurs at 270 °C or more (self-decomposition). If $NaHCO_3$ alone was formed on the working electrode, the cell structure is expressed as

$$Pt|O_2, Na_2O \parallel \text{Na ionic conductor} \parallel NaHCO_3|$$
$$CO_2, O_2, H_2O|Pt \qquad (9)$$

and the cell reactions are expressed as

$$2NaHCO_3 \rightarrow 2Na^+ + 2CO_2 + \tfrac{1}{2} O_2 + H_2O + 2e^- \qquad (10)$$

$$2Na^+ + \tfrac{1}{2} O_2 + 2e^- \rightarrow Na_2O \qquad (11)$$

so the e.m.f. expressed as

$$E = -\left[\frac{\Delta G(Na_2O) + \Delta G(CO_2) - \Delta G(H_2O) - 2\Delta G(NaHCO_3)}{2F}\right] - \frac{RT}{2F} \ln [a(Na_2O)\, P^2(CO_2)\, P(H_2O)] \qquad (12)$$

The activity of Na_2O could be estimated from the result observed in dry test gas for the sensor coated with Na_2CO_3. The e.m.f. can be estimated for the sensor coated with $NaHCO_3$ or NaOH as a function of the water concentration. The results are shown in Fig. 4. For both cases the estimated e.m.f. is considerably higher than for the sensor coated with Na_2CO_3 alone, and it decreases with an increase in water concentration. The results indicate that the e.m.f. of the sensor coated with Na_2CO_3 is increased by the formation of $NaHCO_3$ or NaOH.

3.5. CO_2 sensing characteristics of the sensor with Na_2CO_3 layer

The CO_2 sensing characteristics for a freshly fabricated NA-NGK sensor are shown in Fig. 5a in which the measurement proceeds with an increasing working temperature. The e.m.f. decreased in the initial stage with the holding time at a constant temperature, and the sensitivity to CO_2 was very low in the temperature range below 300 °C. When the temperature was raised to 350 °C or more, the e.m.f. and sensitivity gradually increased with time. Reversible changes of the e.m.f. with CO_2 concentration were observed in a shorter holding time when the temperature increased. Measurement proceeded again after cooling to room temperature in dry air (Fig. 5b). In this case the e.m.f. was higher than that observed below 400 °C in the first measurement. The sensing characteristics observed at 450 °C or more were fairly consistent with the result from the first measurement. A similar characteristic to that of the freshly prepared sensor was observed for a sensor stored in the laboratory atmosphere for more than 5 days. Similar sensing characteristics were also observed in the other sensors, except NA-1000. No reversible sensing characteristic was observed for NA-1000 due to the very porous electrolyte body, as already mentioned, and gas separation between the sensing and reference electrodes could not be achieved.

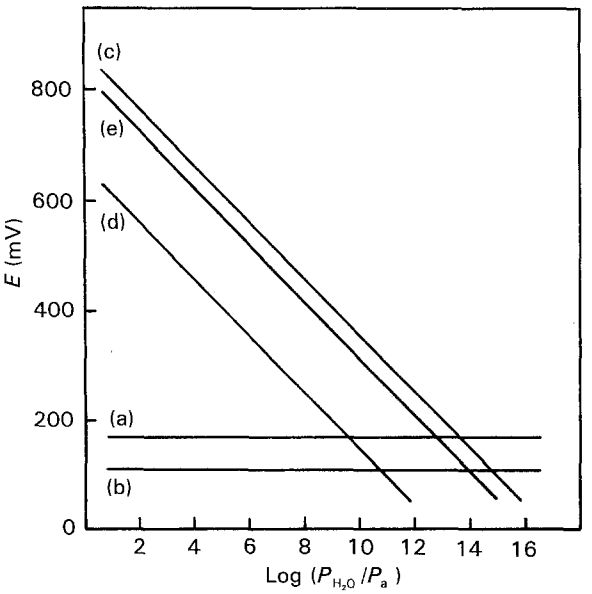

Figure 4 Humidity dependence of the expected e.m.f. at 100 and 1000 p.p.m. CO_2 for the sensor with Na_2CO_3, $NaHCO_3$, or NaOH at 250 °C: (a) element with Na_2CO_3 for 100 p.p.m. CO_2, (b) element with Na_2CO_3 for 1000 p.p.m. CO_2, (c) element with $NaHCO_3$ for 100 p.p.m. CO_2, (d) element with $NaHCO_3$ for 1000 p.p.m. CO_2, (e) element with NaOH for 100 and 1000 p.p.m. CO_2.

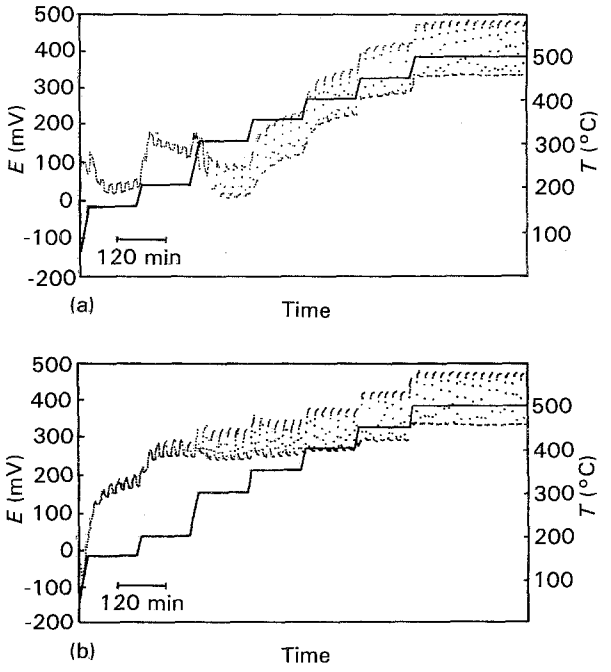

Figure 5 Thermally programmed e.m.f. changes of sensor with NA-NGK during exposure to different concentrations of CO_2 (100 and 10 000 p.p.m.) in dry air: (a) freshly prepared element, (b) element after heating at 500 °C.

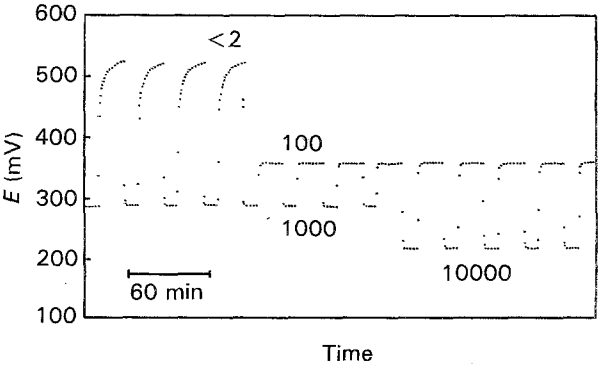

Figure 6 E.m.f. changes of NA-40 during exposure to different concentrations of CO_2 in dry air at 470 °C; the CO_2 concentration in p.p.m. is denoted in the figure.

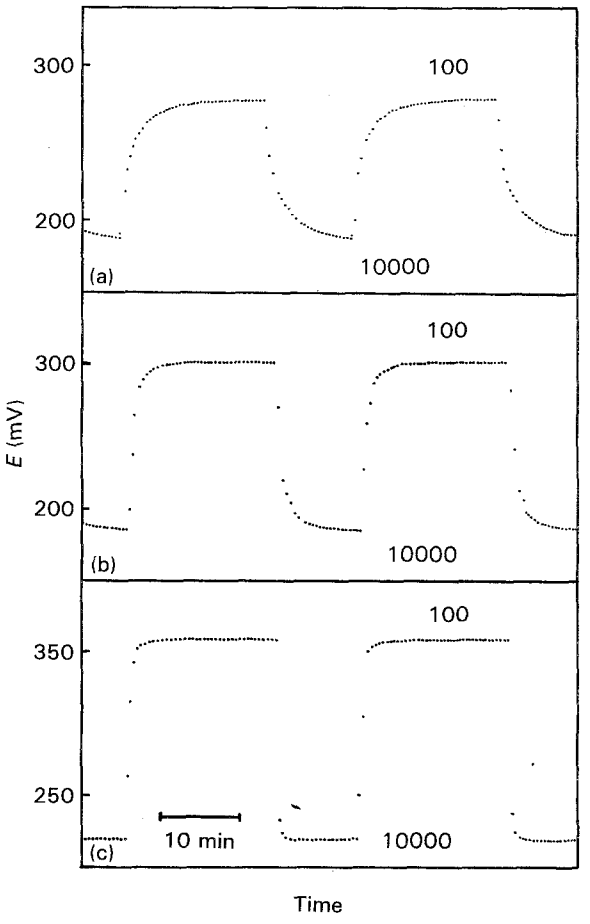

Figure 7 Sensing characteristic of NA-40 at a working temperature of (a) 400 °C, (b) 420 °C, (c) 470 °C. The CO_2 concentration in p.p.m. is denoted in the figure.

The following discussion and description apply to the results observed after stable sensing characteristics were confirmed for a set temperature.

Fig. 6 shows the sensing characteristic at 470 °C for the NA-40 sensor. In this case, air (50 ml min^{-1}) was passed through the reference electrode side. On switching from 1000 p.p.m. CO_2–air flow to just air flow, the e.m.f. increased quickly. A steady state value was not observed within the measuring period (20 min). Except in the case of switching from the air with CO_2 gas to air alone, the rise and recovery times were very fast; the 90% response time was less than 2 min and the rise and recovery times became faster with an increase in the working temperature as shown in Fig. 7. Similar sensing characteristics were also observed for NA-NGK, ZPNA-20 and NAYSI while for NA-1000 no reproducible characteristics were detected.

The two defined characteristics, i.e. the difference in e.m.f. in air and 100 p.p.m. CO_2 ($\Delta E_A = E_{air} - E_{100\ p.p.m.}$) and the sensitivity ($\Delta E$ in mV per decade) are summarized in Table II. It should be noted that $E_{100\ p.p.m.}$ was the value observed in the steady state and E_{air} was the value 20 min after switching from 1000 p.p.m. CO_2 to air and was not the value in the equilibrium state. The sensitivity depends on the temperature and increases with the working temperature, based on the Nernst equation. For all the samples, the observed sensitivity was smaller than the theoretical value and these differences were dependent on the electrolyte species and the working temperature. The number of electrons for the cell reaction was higher than 2, especially at the lower temperature, and approached 2 with an increase in temperature.

In this system the most thermodynamically stable compound is Na_2CO_3, but Na_2O and Na_2O_2 may possibly be formed especially when the concentration of oxygen is high, because of their higher kinetic preference. The possible reactions are as follows:

$$2Na + O_2 \rightarrow Na_2O_2$$

$$2Na + \tfrac{1}{2} O_2 \rightarrow Na_2O$$

$$Na_2O + CO_2 \rightarrow Na_2CO_3$$

$$Na_2O_2 + CO_2 \rightarrow Na_2CO_3 + \tfrac{1}{2} O_2$$

If Na_2O, Na_2O_2 and Na_2CO_3 are formed simultaneously by the cell reactions, the sensitivity may be lower than the theoretical value denoted in Table II, and the galvanic cell will show characteristics of the

mixed potentials given by the relative contributions of the Gibbs energies of formation of the sodium carbonate and the oxides. The decomposition of Na_2O_2 to Na_2O proceeds with an increase in working temperature, and then the sodium oxides react with CO_2, resulting in Na_2CO_3. During the formation of Na_2CO_3 from sodium oxides, the e.m.f. value especially increases with time as observed for freshly prepared sensors in the temperature region 350–450 °C (Fig. 5a). The e.m.f. observed at 400 °C or lower for the sensor pre-heated at 500 °C is considerably higher than that for freshly prepared sensors or sensors stored for a long period in a normal atmosphere. The sensing characteristics observed at 450 °C and above was barely influenced by the history of the sensor.

As shown in Fig. 5a, a decrease in e.m.f. was observed for an initial period after setting the temperature, especially at 350 °C. This is interpreted in terms of the decomposition on NaOH or $NaHCO_3$ to Na_2CO_3, as mentioned. As denoted in Table II, the ΔE_A values for NA-40 were larger by a factor of two than the ΔE values. For the other elements, these values were considerably less. From the e.m.f. in air and the sensitivity estimated in the range between 100 and 10 000 p.p.m., the e.m.f. observed in air corresponded to 3.2 p.p.m. for NA-NGK, 2.0 p.p.m. for NAYSI, 1.8 p.p.m. for ZPNA-20 and 0.37 p.p.m. for NA-40, all operated at 470 °C. The CO_2 content of the air was less than 2 p.p.m., indicating that lower concentrations of CO_2, in the p.p.m. range can be detected by using NA-40. This desirable characteristic may be correlated with the microstructure of the NA-40 body. The response time (especially to air) was not so fast, which may be caused by the decomposition of Na_2CO_3 formed on the sensing electrode (formation of sodium oxides from Na_2CO_3). As described above, NA-40 is composed of both crystalline and glass phases and densification is well advanced (the pore size and surface density of pores are extremely small). Since the two sides of the electrode are completely separated by the densified electrolyte and the electrochemical reaction [5] is limited to the surface of the working electrode side, it is expected that replacement of the test gas is rapidly established by using a densified electrolyte.

3.6. CO_2 sensing characteristics of sensor with $NaHCO_3$ or NaOH layer

To confirm the effects of the existence of an $NaHCO_3$ or NaOH layer, sensing characteristics for the element with an $NaHCO_3$ or NaOH layer were examined. For a freshly prepared element coated with $NaHCO_3$ and then dried at 80 °C, the e.m.f. value rose abruptly when the temperature increased from 150 to 250 °C, while the sensitivity for CO_2 was very small as shown in Fig. 8. At 250 °C the e.m.f. gradually increased and then decreased with the appearance of higher sensitivity. It was clear that the e.m.f. at 250 °C was considerably higher than for the element with Na_2CO_3 (Fig. 9). When the temperature was raised to 350 °C a reversible sensing characteristic could be observed, while a gradual shift (increase) in the e.m.f. was detected in the

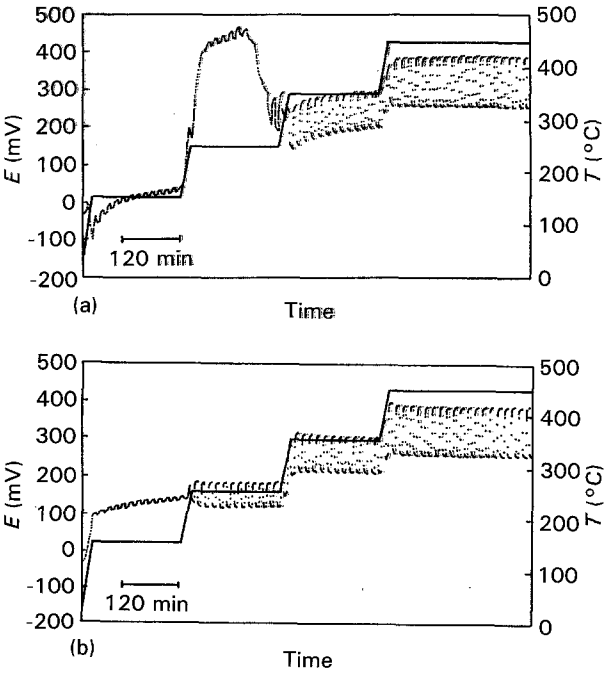

Figure 8 Thermally programmed e.m.f. changes of ZPNA-20 with $NaHCO_3$ during exposure to different concentrations of CO_2 (100 and 10 000 p.p.m.) in dry air: (a) freshly prepared element, (b) element after heating at 500 °C.

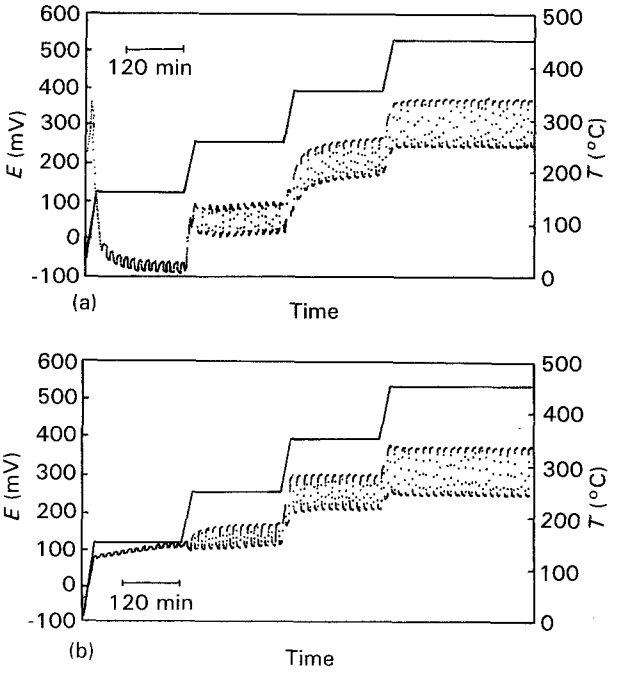

Figure 9 Thermally programmed e.m.f. changes of ZPNA-20 with Na_2CO_3 during exposures to different concentrations of CO_2 (100 and 10 000 p.p.m.) in dry air: (a) freshly prepared element, (b) element after heating to 500 °C.

earlier period after setting the temperature. A similar behaviour was also observed when the temperature was raised to 450 °C. The observed shift (increase) may be caused by the reaction $Na_2O_2 \rightarrow Na_2O \rightarrow (NaHCO_3) \rightarrow Na_2CO_3$, as already mentioned.

In the next measurement, after holding at 450 °C and then cooling to room temperature, a steep rise of e.m.f. was not detected when the temperature was raised from 150 to 250 °C and a stable and reversible sensing characteristic was observed even at 250 °C.

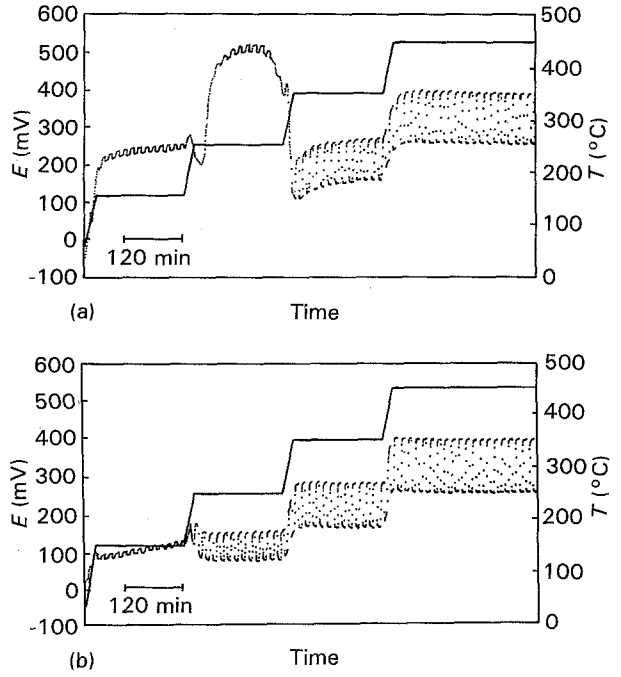

Figure 10 Thermally programmed e.m.f. changes of ZPNA-20 with NaOH during exposure to different concentrations of CO_2 (100 and 10 000 p.p.m.) in dry air: (a) freshly prepared element, (b) element after heating to 500 °C.

The e.m.f. in 100 and 10 000 p.p.m. CO_2 was 198 and 296 mV, respectively, at 350 °C for a freshly prepared element and was comparable to that for the element pre-heated at 450 °C (202 mV in 100 p.p.m. and 303 mV in 10 000 p.p.m.). Furthermore, no distinct differences in e.m.f. were observed at 450 °C.

The sensing characteristics determined at 350 °C or higher for the element with $NaHCO_3$ were also comparable to these for the element with Na_2CO_3. Furthermore, similar results were obtained for the element coated with NaOH instead of Na_2CO_3. The e.m.f. value abruptly increased when the temperature increased from 150 to 250 °C and then decreased as shown in Fig. 10. The sensing characteristics observed at 350 °C or more were also in fair agreement with these for the element coated with $NaHCO_3$ or Na_2CO_3. As previously mentioned, NaOH is a strong getter for CO_2 and reacts with CO_2 forming $NaHCO_3$. $NaHCO_3$ decomposes at 270 °C or more to Na_2CO_3. It seems that the changes in the sensing characteristics caused by the coexistence of $NaHCO_3$ or NaOH in the Na_2CO_3 layer can be removed or recovered when the working temperature is set at 300 °C or more. It is expected that the formation of NaOH or $NaHCO_3$ in the Na_2CO_3 layer induces the enhancement of e.m.f.

3.7. Humidity effects on sensing characteristics

Except for special cases, the gases to be evaluated contained water vapour. Sodium oxides are active toward water molecules and Na_2CO_3 is deliquescent. The characteristic of the NA-40 sensor was barely influenced by the coexistence of the water vapour (15 °C in dew point) at 500 °C (Fig. 11). When the working temperature increased and the water concentration increased to 27 °C in dew point or more, the response time became slower as shown in Figs 12 and 13 for NA-40. The response characteristics are divided into two parts, i.e. the initial first and the following second process. The initial process was hardly influenced by the introduction of water vapour, while the second process was prolonged by the coexistence of water vapour with an increase in temperature. The observation of the second process convinced us of the existence of additional reactions.

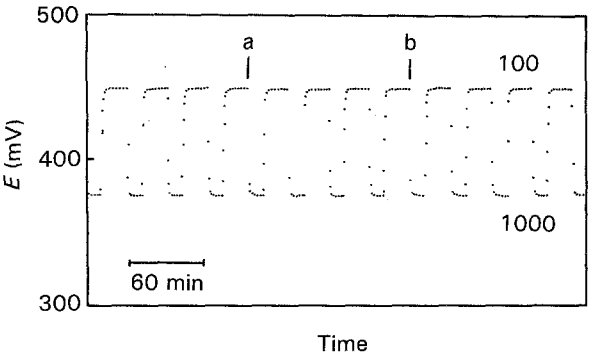

Figure 11 E.m.f. changes of NA-40 during exposures to different concentrations of CO_2 to 500 °C; the CO_2 concentration in p.p.m. is denoted in the figure. Humidification (15 °C in dew point) proceeded in the interval between a and b.

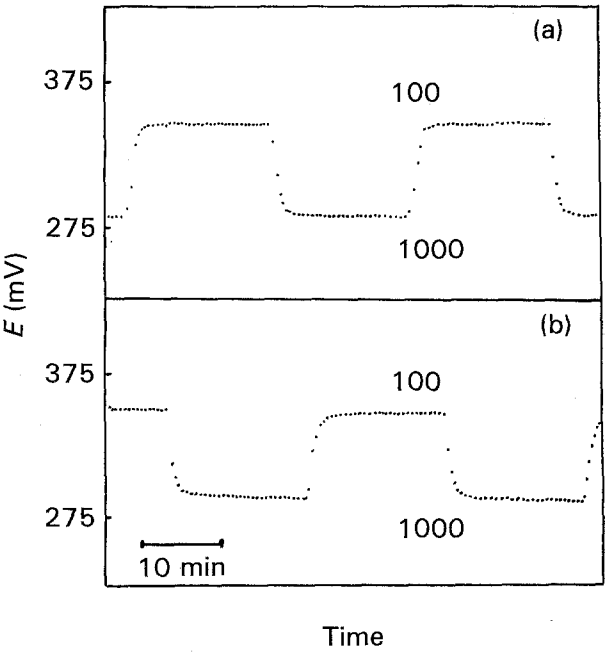

Figure 12 E.m.f. changes of Na-40 at 430 °C (a) in dry air, (b) in wet air (27 °C in dew point). The CO_2 concentration in p.p.m. is denoted in the figure.

The sensitivity and response behaviour changes caused by the humidification were almost completely recovered for NA-40, NA-NGK and ZPNA-20 after switching from humid air to dry air. The e.m.f. values are summarized in Table III. The difference in the e.m.f. values observed in dry and wet air with CO_2 is commonly increased with a decrease in the CO_2 concentration. It is clear that the degree of e.m.f. shift on the introduction of water vapour for $Na_3Zr_2Si_2PO_{12}$-based electrolytes is smaller than for the NAYSI

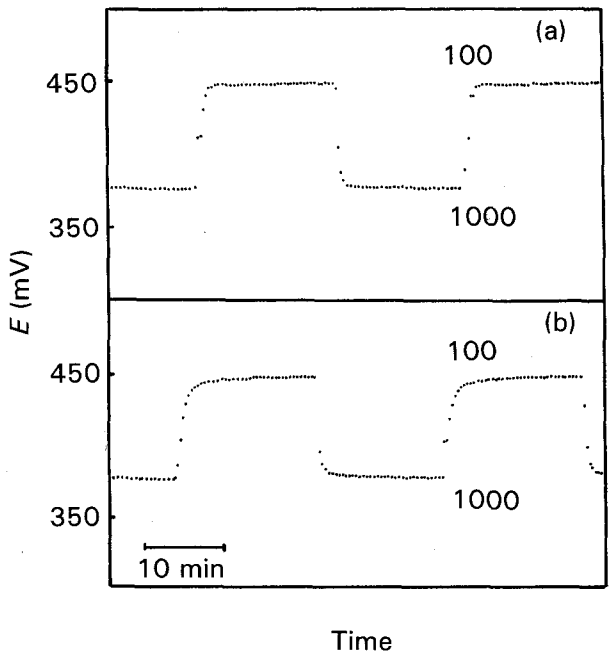

Figure 13 E.m.f. changes of Na-40 at 500 °C (a) in dry air, (b) in wet air (27 °C in dew point). The CO_2 concentration in p.p.m. is denoted in the figure.

TABLE III E.m.f. values for 100 and 1000 p.p.m. CO_2 with and without water vapour

Sample	Temperature (°C)	Dew point (°C)	E.m.f. (mV)[a]	
			100 p.p.m.	1000 p.p.m.
NA-40	470	< −60	416	346
		15	416(0)	346(0)
		27	412(−4)	344(−2)
	500	< −60	448	376
		15	449(+1)	375(−1)
		27	446(−2)	375(−1)
ZPNA-20	460	< −60	341	275
		27	340(−1)	278(+3)
	490	< −60	381	311
		27	377(−4)	310(−1)
NA-NGK	470	< −60	451	378
		27	444(−7)	373(−5)
	500	< −60	482	409
			474(−8)	403(−6)
NYSI	470	< −60	280	208
		15	259(−21)	189(−19)

[a]( ) = Difference from the result observed in dry test gas.

electrolytes. For the NAYSI sensors, the e.m.f. decreased with the introduction of water vapour (15 °C in dew point) and the sensitivity decreased from 72 to 70 mV per decade. The shifts in the e.m.f. were completely recovered after cutting off the water vapour. The introduction of more water (27 °C in dew point) induced a gradual decrease in the sensitivity.

As summarized in Table III, the extent of the decrement in e.m.f. increased with the humidity and with a decrease in CO_2 concentration. If surface NaOH or $NaHCO_3$ is formed, the e.m.f. may be higher than that observed in dry air, since the e.m.f. value for the sensor having NaOH or $NaHCO_3$ is higher than that for the sensor coated with Na_2CO_3 as mentioned. Prolongation of the response time and a decrease in the e.m.f. due to the coexistence of water vapour are at least qualitatively realized by the following reactions and not by the formation of surface NaOH or $NaHCO_3$:

$$Na_2CO_3 + H_2O \rightarrow 2Na^+ + CO_3^- \quad \text{(dissociation)}$$

$$2Na^+ + XO_2 \rightarrow Na_2O_X \quad \text{(e.m.f. decrease)}$$

$$Na_2O_X + CO_2 \rightarrow Na_2CO_3 \quad \text{(e.m.f. recovery)}$$

When the sensor is heated to 270 °C or more, it seems that the e.m.f. drift caused by the formation of Na_2O_X can be stopped by cutting off the water vapour supply, since Na_2O_X reacts with CO_2 forming $NaHCO_3$ which decomposes to Na_2CO_3 and H_2O. If the formation of sodium oxides is limited on the surface of the electrolyte, recovery proceeds easily and quickly. Actually, the recovery of sensitivity observed after cutting off the water vapour was very fast.

4. Conclusions

Based on these results, the following clarifications have been made:

1. For the $Na_3Zr_2Si_2PO_{12}$-based electrolyte, no distinct increase in weight on exposure to humid air, with or without CO_2 species, was observed. The resistivity at 300 °C or more was hardly influenced by the ambient conditions.
2. The electron number of the reaction was higher than 2 and approached 2 with an increase in the working temperature for electrochemical CO_2 gas sensors.
3. The sensitivity and the response behaviour were satisfactory when the densified sensor was operated at 470 °C. The e.m.f. decreased slightly and the response times were prolonged when water vapour (27 °C in dew point) was introduced. The characteristics recovered almost completely after the cutting off of water vapour. The e.m.f. lowering by water sorption was depressed by using a densified $Na_3Zr_2Si_2PO_{12}$.

References

1. J. B. GOODENOUGH, H. Y. P. HONG and J. A. KAFALS, *Mater. Res. Bull.* **11** (1976) 203.
2. U. VON ALPEN, M. F. BELL, R. BRÜTIGAN and H. LAIG-HÖRSTEBROCK, in "Fast Ion Transport in Solids", edited by M. V. Vashista, J. N. Mundy and G. K. Shenoy (North-Holland, Amsterdam, 1979) p. 443.
3. C. C. HUNTER and M. D. INGRAM, *Solid State Ionics* **14** (1984) 31.
4. M. S. NIEUWENHUIZEN and A. J. NEDERLOF, *Sensors and Actuators* **B2** (1990) 97.
5. M. NAGAI, T. SAEKI and T. NISHINO, *J. Amer. Ceram. Soc.* **73** (1990) 1456.
6. O. H. LeBLANC Jr, W. J. WARD, S. L. MATSON and S. G. KIMURA, *J. Membrane Sci.* **6** (1980) 339.
7. M. GAUTHIER and A. CHAMBERLAND, *J. Electrochem. Soc.* **124** (1977) 1579.
8. G. HÖ TZEL and W. WEPPNER. *Solid State Ionics.*, 18/19, (1986) 1223.

9. R. AKILA and K. T. JACOB. *J. Appl. Electrochem.* **18** (1988) 245.
10. S. YAO, Y. SHIMIZU, N. MIURA and N. YAMAZOE, *Chem. Lett.* (1990) 2033.
11. Y. SAITO, T. MARUYAMA, Y. MATSUMOTO and Y. YANO, in Proceedings of International Meeting on Chemical Sensors, 19–22 September 1983, (Kodansha Elsevier, 1983) p. 326.
12. J. LIU and W. WEPPNER, *Solid State Commun.* **76** (1990) 311.
13. N. IMANAKA, T. KAWASATO and G. ADACHI, *Chem. Lett.* (1990) 497.
14. Y. SADAOKA and Y. SAKAI, *J. Mater. Sci.* **20** (1985) 3027.
15. B. DUNN, *J. Amer. Ceram. Soc.* **64** (1981) 125.

Received 1 July 1992
and accepted 27 April 1993